Collectivization of anti-analog strength above charged particle thresholds

J. Okołowicz,[1] M. Płoszajczak,[2] R. J. Charity,[3] and L. G. Sobotka[3]
[1]*Institute of Nuclear Physics, Radzikowskiego 152, PL-31342 Kraków, Poland*
[2]*Grand Accélérateur National d'Ions Lourds (GANIL), CEA/DSM CNRS/IN2P3, Boîte Postale 55027, F-14076 Caen Cedex, France*
[3]*Departments of Chemistry and Physics, Washington University, St. Louis, Missouri 63130, USA*

(Received 19 November 2017; published 9 April 2018; corrected 12 April 2018)

Ten years ago, highly excited states were found in ^{9}Li and ^{10}Be a few hundred kilovolts above the proton decay threshold. These physical states are too low in energy to be the isospin-stretched configuration of the decay channel (the isobaric analog or $T_>$). However, these states can be understood by a continuum cognizant shell model as strongly mixed states of lower isospin ($T_<$), where the mixing is largely mediated by the open neutron channels but ushered in energy to be just above the proton threshold.

DOI: 10.1103/PhysRevC.97.044303

I. INTRODUCTION

Some of the most critical steps in the making of the elements (nucleosynthesis) are enabled by the fortuitous occurrence of resonances in the composite system very close to the combined mass of the reactants. Two examples are the Hoyle state in ^{12}C just above the $\alpha + {}^{8}$Be entrance channel [1], where a decay branch to particle-bound carbon forms the seeds for the synthesis of heavier elements, and a resonance in ^{17}O within 3 keV of the $\alpha + {}^{13}$C threshold where a neutron-decay branch enables the slow neutron-capture process. The apparent tuning of these resonances in synthetic paths is consistent with an anthropic argument [2,3]. Here we discuss resonances not on any synthetic path; i.e., they are divorced from anthropic logic and a basic science explanation must be found for their existence.

About a decade ago two high-lying resonances were found by invariant-mass spectroscopy, one in ^{9}Li and the other in ^{10}Be, just above the opening of their respective proton-decay channels [4]. The energies of these resonances were well above the respective thresholds for neutron decay. In both cases, the resonance energies were close to, but below, where one expected the isospin-stretched ($T_>$) mix of the proton and its decay partner ($^{8}\mathrm{He}_{\mathrm{g.s.}}$ for the ^{9}Li* resonance and $^{9}\mathrm{Li}_{\mathrm{g.s.}}$ for the ^{10}Be* case). If the energies had been consistent with the isospin-stretched expectations, claims would have been made for the discovery of the isobaric analog states (IASs) of ^{9}He and ^{10}Li. As this was not the case, the experimental work concluded without a satisfactory explanation of these resonances.

One of the most significant advances in nuclear theory in the past decade has been in constructing structure models that realistically incorporate the near continuum, such as the Gamow shell model [5–7], the complex-energy continuum shell model (CSM) based on the Berggren ensemble [8], and the real-energy CSM [9,10] based on the projection formalism [11,12]. It has been shown that the interaction of shell model (SM) states with the continuum can lead to resonance trapping [13,14], super-radiance phenomena [15], multichannel coupling of shell occupancies [16], or the generation of states close to, and with a significant spectroscopic overlap with, a decay channel [17–19]. The term "collectivization" is used to refer to the latter case, i.e., continuum-mediated configuration mixing that generates physical states with spectroscopic properties similar to—and close to the energy of—a particle-decay channel, and it is this type of phenomenon that explains the resonances observed a decade ago in ^{9}Li and ^{10}Be. These cases are interesting for two reasons. First, while the states are close to the charged-particle threshold, it is the neutron continuum that generates the width of the states and is a significant factor in the mixing and in the ushering of the resonance energy toward the charged-particle threshold. The second reason the near-threshold resonances in ^{9}Li and ^{10}Be are interesting is that they have the same spin and parity as the IAS but are $T_<$. Therefore, in these cases, the continuum-mediated mixing (or collectivization) occurs within the fractured anti-analog strength. The unfractured antianalog state (AAS) has the same component structure of the IAS but with an isospin antiparallel configuration of its clustered components [20,21].

Although these resonances were presented previously [4], this work presents an improved experimental analysis. We then explain these resonances with SM calculations that incorporate *both* the open proton and neutron channels.

II. EXPERIMENTAL METHODS

The resonances were reconstructed from high-resolution measurements of the relative energy between the decay fragments: $^{9}\mathrm{Li}^* \rightarrow p + {}^{8}$He and $^{10}\mathrm{Be}^* \rightarrow p + {}^{9}$Li. Because this experiment was fully described previously [4], it is only briefly described here. A secondary ^{12}Be beam (intensity of 1×10^{5} s^{-1} and purity of 87%) was generated by the Coupled Cyclotron Facility at the National Superconducting Cyclotron Laboratory at Michigan State University using a primary ^{18}O beam of $E/A = 120$ MeV and a Be target. Reactions of the secondary beam on polyethylene and carbon targets (thicknesses of 1.0 and 0.4 mm, respectively) were studied with the charged-particle detection array HiRA [22] and composite spectra from both targets are presented. In this experiment, HiRA consisted of 16 Si-CsI(Tl) telescopes located 60 cm downstream of the

TABLE I. Resonance data (left) and shell model embedded in the continuum complex eigenenergies (right) for ^{9}Li $J^{\pi}_{n} = 1/2^{+}_{n}$ ($3 \leqslant n \leqslant 6$) and ^{10}Be $J^{\pi}_{n} = 2^{-}_{n}$ ($10 \leqslant n \leqslant 14$) and $J^{\pi}_{n} = 1^{-}_{n}$($n = 9,10$) states. Both total and proton calculated decay widths are provided. For the former all decay channels indicated in Fig. 2 are coherently included.

Data			Calculations					
E^{*} (MeV)	E_p (MeV)	Γ (keV)	J^{π}	n	E^{*} (MeV)	E_p (MeV)	Γ (keV)	Γ_p (keV)
				^{9}Li				
			$\frac{1}{2}^{+}$	3	11.04	−2.90	60	0
			$\frac{1}{2}^{+}$	4	12.35	−1.59	61	0
14.104(17)	0.160(17)	75(10)	$\frac{1}{2}^{+}$	5	14.09	0.15	75[a]	1.9
			$\frac{1}{2}^{+}$	6	14.62	0.68	47	0.7
				^{10}Be				
			2^{-}	10	19.85	0.21	155	0.1
			2^{-}	11	20.16	0.52	142	1.9
20.38(3)[b]	0.74(3)	358(30)	2^{-}	12	20.38	0.74	181	14
			1^{-}	9	20.82	1.18	278	3.1
			2^{-}	13	21.13	1.50	185	7.6
21.18(3)[c]	1.54(3)	272(90)	2^{-}	14	21.30	1.66	102	18
			1^{-}	10	21.36	1.72	328	0.8

[a]Fixed by choice of V_0.
[b]Has a weak low-energy shoulder.
[c]Member of a multiplet.

target. The telescopes were arranged in four towers of four telescopes each, with two towers on each side of the beam. The array subtended the angular region $2.7^{\circ} < \theta < 24.8^{\circ}$. Each telescope consisted of a 1.5-mm-thick, double-sided Si-strip (ΔE) detector (each side with 32 strips) followed by four 4-cm-thick CsI(Tl) stopping (E) detectors arranged in quadrants. Signals produced in the 1024 Si strips were processed with HINP16C chip electronics [23]. The silicon detectors were calibrated using α sources and the CsI(Tl) detectors calibrated using cocktail beams. Simulations of the device response incorporated each element's energy and position resolution, the beam spot size, and multiple scattering in the target.

The present investigation prompted an improved analysis as compared to that performed in Ref. [4]. While an upgraded CsI(Tl) energy calibration improved the resolution of the total invariant-mass spectra, here we have chosen to examine events whose decay axis is approximately perpendicular to the beam axis as these events have better detector resolution. The line shapes of the resonances were first fit using the R-matrix formalism for a single proton channel (no competing neutron channels) [24]. However, if the proton branching ratio is small (as is the case), a more appropriate form is a Breit-Wigner line shape times the proton penetration factor. The fitted centroids and widths obtained from both approaches are similar and the reported results (Table I) represent averages with an error encompassing the statistical uncertainties of both. The invariant-mass reconstructions for ^{9}Li* and ^{10}Be* are shown in Figs. 1(a) and 1(b), respectively.

III. EXPERIMENTAL RESULTS

A. ^{9}Li*

^{9}Li has a narrow resonance at $E^{*}_{1} = 14.104(17)$ MeV, 160 keV above the $p + ^{8}$He threshold, with a width of $\Gamma_1 = 75(10)$ keV. The p-^{8}He angular correlation (decay axis relative to the beam direction) is consistent with s-wave emission, but due to the marginal statistics for an angular distribution of the resonance data, p-wave emission cannot be excluded. This experimental difficulty does not lead to an ambiguity as the calculations indicate that there are no states of the opposite parity near the proton-decay threshold. The energy of this resonance is lower than that expected for the IAS $T = 5/2$. No narrow resonances are observed at higher energies; however, there is broad strength near $E^{*}_{2} \sim 16$ MeV, for which its width is not well constrained due to uncertainty in the background. This strength could be one or more $T = 3/2$ states (of which there should be many) or the IAS, the analog of ^{9}He ($T = 5/2$). The latter interpretation is consistent with recent $p + ^{8}$He scattering results [25]; however, we favor the former explanation for reasons to be mentioned later.

B. ^{10}Be*

The reconstruction of ^{10}Be presents several features: a peak at $E^{*}_{1} = 20.38(3)$ MeV with $\Gamma_1 = 358(30)$ keV that requires a weak low-energy shoulder for a good fit, and broad strength near 21.5 MeV for which a multiplet is required to obtain an acceptable fit of which only the lowest-energy member, at $E^{*}_{2} = 21.18(3)$ MeV and $\Gamma_2 = 272(90)$ keV, is constrained by these data. Although three states are shown to contribute to this multiplet in Fig. 1(b), reasonable fits can be obtained with two or more states.

A resonance at 21.2 MeV was observed previously and was tentatively assigned as the IAS ($T = 2$) [26]. This (tentative) assignment preceded any information on the analogs. We now know that the ground state of ^{10}Li is essentially at the neutron threshold (Δ (^{10}Li) ~ 33.0 MeV) [27] and recent work has also placed the ground state of ^{10}N unbound by

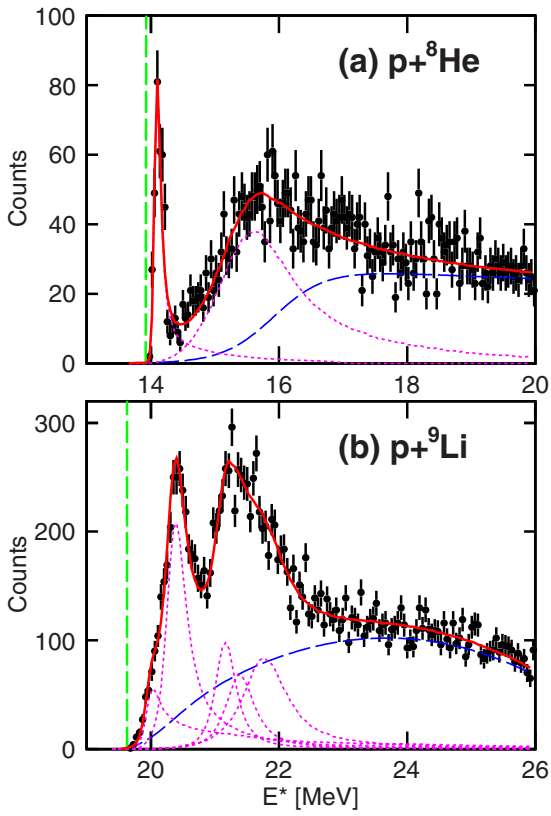

FIG. 1. Invariant-mass reconstructions of (a) ^{9}Li* and (b) ^{10}Be* from the indicated decay channels. The vertical lines are the proton-decay thresholds (13.944 and 19.636 MeV) and the dotted (dashed) curves indicate the fitted states (backgrounds).

1.9–2.2 MeV ($\Delta(^{10}\mathrm{N}) = 38.1$–$38.4$ MeV) [28]. The $A = 10$, $T = 1$, and $J^{\pi} = 0^{+}$ states and a sharp-sphere uniform-charge model provide estimates of the linear (b) and quadratic (c) isobaric multiplet mass equation parameters [29,30]. If the $T = 1$ values for b and c are retained for the $T = 2$ levels and the offset parameter, a, is adjusted to reproduce the ground states of the $|T_z| = 2$ states (mentioned above), the excitation energy of the IAS in ^{10}Be is between 23.4 and 24.5 MeV. (Reference [31] provides an application of this logic.) The limits come from extrapolations from ^{10}N ($J^{\pi} = 2^{-}$) and ^{10}Li, respectively. (The lower value drops to 23.1 MeV if the ground state for ^{10}N is $J^{\pi} = 1^{-}$; see Ref. [28].) While the isobaric multiplet mass equation can have deviations and the method of parameter determination is simplistic, the employment of information on both (isospin projection) sides suggests that all the peaks in ^{10}Be below 22 MeV [all structures shown in Fig. 1(b)] result from $T = 1$ states.

IV. CONTINUUM-SHELL-MODEL FORMALISM

The calculations are performed using the shell model embedded in the continuum (SMEC) [9,32,33]. The theory has been presented in full [9,17,18] and here we only repeat the features relevant for understanding the nature of the collectivization of the near-resonance states. The Hilbert space is divided into two orthogonal subspaces $\mathcal{Q}_0$ and $\mathcal{Q}_1$ containing zero particles and one particle in the scattering continuum, respectively. An open quantum system description of $\mathcal{Q}_0$ space includes couplings to the environment of decay channels through the energy-dependent effective Hamiltonian: $\mathcal{H}(E) = H_{\mathcal{Q}_0\mathcal{Q}_0} + W_{\mathcal{Q}_0\mathcal{Q}_0}(E)$. $H_{\mathcal{Q}_0\mathcal{Q}_0}$ denotes the standard SM Hamiltonian describing the internal dynamics in the closed quantum system approximation, and $W_{\mathcal{Q}_0\mathcal{Q}_0}(E) = H_{\mathcal{Q}_0\mathcal{Q}_1} G^{(+)}_{\mathcal{Q}_1}(E) H_{\mathcal{Q}_1\mathcal{Q}_0}$ is the energy-dependent continuum-coupling term, where $G^{(+)}_{\mathcal{Q}_1}(E)$ is the one-nucleon Green's function and $H_{\mathcal{Q}_0,\mathcal{Q}_1}$ and $H_{\mathcal{Q}_1\mathcal{Q}_0}$ are the coupling terms between the orthogonal subspaces $\mathcal{Q}_0$ and $\mathcal{Q}_1$. E in the above equations stands for a scattering energy. The energy-dependent coupling term can also be written $W_{\mathcal{Q}_0\mathcal{Q}_0}(E) = V_0^2 h(E)$, where V_0 is the continuum-coupling strength and $h(E)$ is the coupling term between localized states in $\mathcal{Q}_0$ and the environment of one-nucleon decay channels in $\mathcal{Q}_1$. In this work, the parameter V_0 is adjusted to reproduce the width of the near-threshold resonance in ^{9}Li*; all other parameters in the interaction were left at the literature values. The zero of the energy scale for each particle type is fixed at the lowest corresponding one-nucleon emission threshold and the decay channels of nucleus A are defined by the coupling of one nucleon (proton or neutron) in the continuum to nucleus $A - 1$ in a given SM state.

SMEC solutions in $\mathcal{Q}_0$ are found by solving the eigenproblem for the non-Hermitian effective Hamiltonian $\mathcal{H}(E)$ [9,18]. The complex eigenvalues of $\mathcal{H}(E)$ at energies $E_j(E) = E$ determine the energies and widths of resonance states. In a bound system ($E < 0$), the eigenvalues of $\mathcal{H}(E)$ are real. In the continuum, $E_j(E)$ correspond to the poles of the scattering matrix. Eigenstates $|\Psi_j\rangle$ of $\mathcal{H}(E)$ are linear combinations of SM eigenstates $|\psi_i\rangle$ generated by the orthogonal transformation matrix $[b_{ji}(E)]$, where squared matrix elements $b^2_{ji}(E)$ are weights of the SM eigenstate i in the SMEC eigenstate j at the energy E. Continuum-induced mixing of SM eigenstates is particularly strong if several avoided crossings of SMEC eigenstates appear [9,17,18]. These crossings can be studied by calculating either energy trajectories of the double poles of the scattering matrix for $\mathcal{H}(E)$ with the complex-extended continuum-coupling strength [34], or the continuum-coupling correlation energy, $E^{(j)}_{\mathrm{corr}}(E) = \langle\Psi_j|W_{\mathcal{Q}_0\mathcal{Q}_0}(E)|\Psi_j\rangle$, for the SMEC eigenstate Ψ_j, i.e., the expectation value of the continuum-coupling term in the SMEC eigenstate Ψ_j. Above the particle emission threshold ($E > 0$), $\langle\Psi_j|W_{\mathcal{Q}_0\mathcal{Q}_0}(E)|\Psi_j\rangle$ is complex and, hence, $E^{(j)}_{\mathrm{corr}} = \mathrm{Re}[\langle\Psi_j|W_{\mathcal{Q}_0\mathcal{Q}_0}(E)|\Psi_j\rangle]$.

Making an analogy to BCS theory, the continuum-coupling energy is analogous to the expectation value of the pairing interaction term in the BCS Hamiltonian, or Δ^2/G, where G is the pairing strength. These are not the change in the total energy due to the included physics. In the BCS case this energy shift can be calculated by the difference between the BCS and Hartree-Fock ground-state energies. There is no obvious analogy for this energy shift for the present continuum problem as the induced correlations affect all SM states.

The scattering energy for which the continuum-induced mixing of the SM eigenstates is the strongest generates a minimum in $E^{(i)}_{\mathrm{corr}}(E)$ [17,18]. A state near this minimum not only benefits from the continuum-mediated mixing, but also carries many features of the nearby decay channel. The energy

where this effect (which we call collectivization) is strongest is determined by a subtle interplay between the competing forces of repulsion (Coulomb and centrifugal interaction) and attraction (the continuum coupling), and only for the coupling to the $l = 0$ neutron-decay channel is it precisely at the threshold [34]. Detailed discussion of the continuum-coupling-induced collectivity in near-threshold states is given elsewhere [17,18].

The SM Hamiltonian uses the recently developed monopole-based interaction for the full *psd* model space that includes (0–3)$\hbar\omega$ excitations [35]. We refer to this interaction as YSOX and it has been quite successful in reproducing ground-state properties of *psd* nuclei from drip line to drip line. YSOX is supplemented by the Wigner-Bartlett contact interaction for the coupling between the SM states and the decay channels. The standard value of spin-exchange parameter ($\beta = 0.37$) is used.

The radial single-particle wave functions in $\mathcal{Q}_0$ and the scattering wave functions in $\mathcal{Q}_1$ are generated using a Woods-Saxon (WS) potential which includes spin-orbit and Coulomb parts. The radius and diffuseness of the WS potential are $R_0 = 1.27A^{1/3}$ fm and $a = 0.67$ fm, respectively. The spin-orbit potential is $V_{SO} = 6.4$ MeV, and the Coulomb part is calculated for a uniformly charged sphere with radius R_0. The depth of the central part for protons (neutrons) in ^{9}Li and ^{10}Be is adjusted to yield the energy of the $p_{3/2}$ proton (neutron) single-particle state equal to the one-proton (one-neutron) separation energy in the ground state of ^{9}Li and ^{10}Be. Two-body Coulomb interaction is absent in YSOX interaction; hence, the SM eigenstates have good isospin. However, one-nucleon decay channels do not have good isospin so the coupling to decay channels induces isospin nonconservation in the SMEC eigenstates. Our state notation is J^π_n and T for the spin, parity (superscript), the ordinal label for that spin (subscript), and isospin of the largest SM component of the SMEC eigenstate. The calculated level diagrams, only including the states of relevance for the present study, are shown in Fig. 2.

V. CONTINUUM-SHELL-MODEL RESULTS

A. ^{9}Li*

The YSOX interaction predicts two $J^\pi_n = 1/2^+$ ($n = 5,6$), $T = 3/2$, states just above the proton-emission threshold at 13.94 MeV [see Fig. 2(a)]. The second of these is predicted to have a tiny proton partial decay width. The $J^\pi_n = 1/2^+_5$ resonance has the energy of the observed resonance and if the strength of the continuum-coupling interaction is fixed at $V_0 = -208(\pm 14)$ MeV fm^3 (and all decay channels shown in Fig. 2 are included), the experimental width is reproduced. The parametric uncertainty comes from the experimental uncertainty of the resonance width. The partial proton width is only $\Gamma_p = 1.9\,(\pm 0.4)$, (± 0.5) keV, where the uncertainties come from those of V_0 and the resonance position, respectively. With the SMEC energy scale origin as the experimental proton-emission threshold, the ground-state energy of ^{9}Li is –13.86 MeV, 0.08 MeV less bound than reality (by 0.6%).

The proton $s_{1/2}$ spectroscopic factor for the $J^\pi_n = 1/2^+_5$ state is 0.14. This is the second largest spectroscopic factor among all $J^\pi = 1/2^+, T = 3/2$ states. Large spectroscopic factors are the hallmark of the continuum-induced collectivization. (The wave-function components of all relevant states can be found in the tables provided in the Supplemental Material [36].)

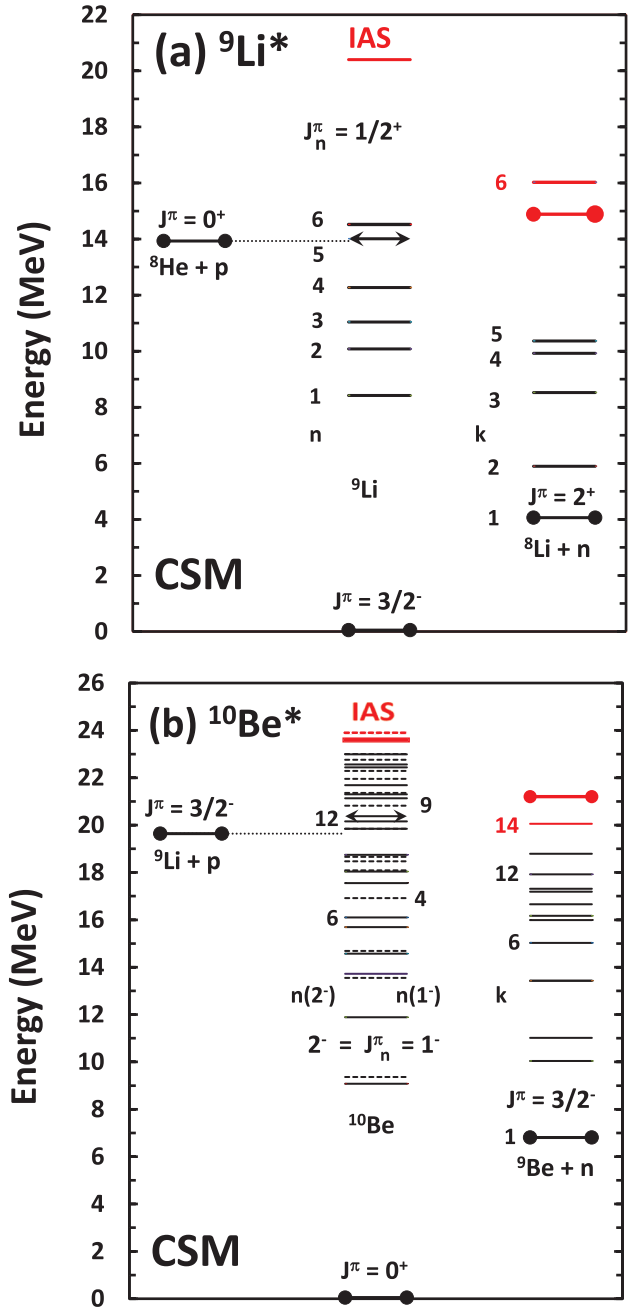

FIG. 2. Continuum-shell-model level diagrams for relevant (a) ^{9}Li* and (b) ^{10}Be* resonances. All shown levels are coherently coupled in the SMEC calculations. The black (red) lines indicate $T_<$ ($T_>$) levels, lines with end points are experimental levels, and those with arrows indicate the lowest-lying levels with a significant proton-decay branch. The ^{9}Li levels of $J^\pi = 1/2^+$, ^{10}Be levels with $J^\pi = 2^-$ (solid lines) and 1^- (dashed lines), the ground-state proton decay channel, and the relevant n-decay channels are all indicated. The wave-function compositions are provided in the supplementary tables that are organized by the indices n and k [36].

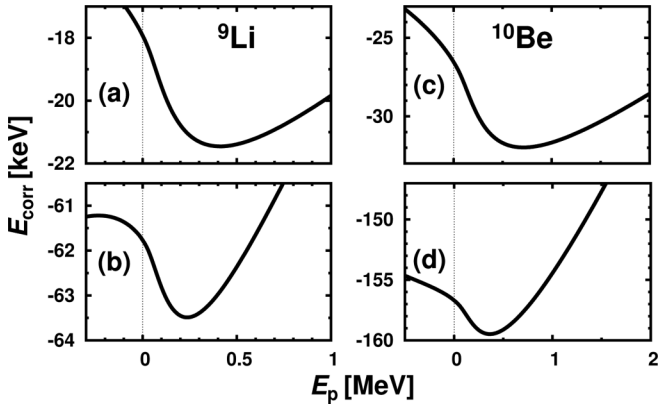

FIG. 3. The continuum-coupling correlation energy as a function of proton energy E_p for (a) $J^\pi = 1/2^+$, $T = 3/2$ SM states with an excitation energy $E^* < 15$ MeV coupled in s wave to the (lowest) one-proton decay channel and (b) with the additional coupling to all one-neutron decay channels, and (c) ^{10}Be* for the $J^\pi_n = 2^-_{12}$, $T = 1$ state considering all $J^\pi = 2^-$, $T = 1$ SM states with an excitation energy $E^* < 22$ MeV s wave coupled to the (lowest) one-proton decay channel and (d) with the addition of coupling to nine neutron-decay channels.

As mentioned above, a metric for the degree of mixing of SM states, due to the continuum, is the continuum-coupling correlation energy $E_{\rm corr}$. Figure 3(a) shows the collectivization for $J^\pi = 1/2^+, T = 3/2$ SM eigenstates due to coupling to the $p + {}^8$He decay channel. Convergence is achieved when all SM states with the excitation energy $E^* \leqslant 16.1$ MeV are taken into account. With only this single decay channel included, the centroid of the opportunity energy window for a collective near-threshold state is above the observed energy of the resonance. Figure 3(b) shows what happens to $E_{\rm corr}$ when coherent couplings to *all* the open neutron-decay channels shown in Fig. 2 are also included. The optimal energy for collectivization shifts down to $E_p \sim 0.24$ MeV, in this case very close to coinciding with the position of the physical resonance.

While not the subject of the present work, these calculations do indicate that the ground state of ^{9}He is $J^\pi = 1/2^+$ and the first excited state is $J^\pi = 1/2^-$. The IAS in ^{9}Li ($J^\pi = 1/2^+$, $T = 5/2$) is found at 20.4 MeV in the SM calculation and, as expected, the neutron $s_{1/2}$ and proton $s_{1/2}$ wave-function components are in the expected isospin Clebsch-Gordan ratio of 4:1. (That is the square of $\langle 2,1;\frac{1}{2},\frac{1}{2}|\frac{5}{2},\frac{3}{2}\rangle/\langle 2,2;\frac{1}{2},-\frac{1}{2}|\frac{5}{2},\frac{3}{2}\rangle$, for a neutron coupled to the IAS of ^{8}Li relative to a proton coupled to ^{8}He.) This state is close to the inelastic one-proton emission channel [$p + {}^8$He($E^*_{\rm expt} = 6.03$ MeV)] in ^{9}Li. The coupling of the IAS state to the lowest one-proton emission channel, its isobaric analog in ^{8}Li, and inelastic proton emission channels (the known $J^\pi_n = 2^+_1$ and 1^-_1 states in ^{8}He and even an unknown $J^\pi_n = 2^-_1$) do not significantly change the energy and yield the total width of less than 50 keV; interestingly this is primarily from the proton partial width. While the partition between neutron and proton widths is sensitive to the ratio of the continuum-coupling constants for like and dissimilar nucleons, the total width is largely unaffected by this ratio. While a measurement of the n/p-decay branching ratio would help fix this ratio, we conclude (unless an important ingredient is missing in our effective Hamiltonian) that the wide structure attributed to the ^{9}Li IAS [25] is unlikely to be solely $T = 5/2$.

Returning to the near-threshold state, $J^\pi_n = 1/2^+_5$ (and for that matter the subthreshold $J^\pi_n = 1/2^+_3$), its wave function has the neutron-to-proton s-component strengths swapped relative to the IAS; i.e., the proton s component exceeds the neutron s component. This is expected from the isospin Clebsch-Gordan coefficients for an anti-analog $T_<$ state. (Here one is coupling the nucleon and residual to $T = \frac{3}{2}$ with the same projection.)

B. ^{10}Be*

Near the ^{10}Be proton-decay threshold (19.6 MeV), five $J^\pi_n = 2^-$, $T = 1$ ($10 \leqslant n \leqslant 14$) states and two $J^\pi_n = 1^-$, $T = 1$ ($n = 9,10$) states are predicted [see Table I and Fig. 2(b)]. These SM states are mixed strongly through the coupling to the proton-emission channel and all but one have proton partial decay widths which are sufficiently large to be seen experimentally. The energy of the $J^\pi_n = 2^-_{12}$, $T = 1$ state coincides with the observed resonance [see Table I and Fig. 1(b)]. The proton-partial-decay width for this state is the second largest among all $J^\pi_n = 1^-, 2^-$ states within 2 MeV of the proton-emission threshold and its $s_{1/2}$ spectroscopic factor is the largest (0.11) among all considered $J^\pi = 1^-, 2^-$ states. Both $J^\pi_n = 1^-_9$ and 1^-_{10} states are broad and have small proton-partial-decay widths but should contribute to the tails of observed peaks.

The continuum-coupling correlation energies for the $J^\pi_n = 2^-_{12}$ eigenstate obtained by considering coupling to proton, and proton- and neutron-decay channels are shown are Figs. 3(c) and 3(d), respectively. The proton energy where $E_{\rm corr}$ is optimal, i.e., where the collectivization of the SM wave function is the strongest, coincides with the energy of the observed low-lying state when the proton channel is considered. With the inclusion of neutron channels, the overall collectivization increases and the centroid of the opportunity energy window for collectivization moves even closer to the proton-emission threshold. The ground-state energy of ^{10}Be is calculated to be at –18.74 MeV, again under bound, this time by 0.9 MeV (4.6%).

This collection of states provides a remarkable reproduction of what is observed: a narrow low-energy peak with a higher-energy broad structure that is clearly a multiplet. Even the requirement of a weak component on the low-energy side of the prominent structure nearest threshold finds an explanation (see Table I). The fact that the individual calculated widths are smaller than the extracted widths is to be expected due to the multiplicity of eigenstates (with the same quantum numbers) in the energy region just above the proton threshold.

The IAS ($T = 2$) in ^{10}Be is either $J^\pi = 2^-$ or 1^- and these states are predicted to be at 23.6 and 23.9 MeV, respectively. Their energies are close to the threshold of an inelastic one-proton emission channel [$p + {}^9$Li($E^*_{\rm expt} = 4.3$ MeV)]. Both states, when coupled to the lowest-lying $J^\pi = 3/2^-$, $1/2^-$, and $5/2^-$ one-proton emission channels and their isobaric analogs ($T = 3/2$) in ^{9}Be, shift to higher energies, 24.7 and 25 MeV, and acquire total (proton partial) widths of 99 (53)

and 85 (62) keV, respectively. These energies are close to where they are expected to be based on the now known energies of other members of the isobaric multiplet. The most important channels for IAS decay are to the first $J^\pi = 3/2^-$, $T = 3/2$ levels in ^{9}Li and ^{9}Be.

VI. SUMMARY

In the case of ^{9}Li* the continuum-induced mixing of SM states, which we have been calling "collectivization," for $J^\pi = 1/2^+$, $T = 3/2$ becomes stronger when neutron channels are considered and optimal just above the proton threshold where the resonance is observed. While the predicted spectrum is complex for the ^{10}Be* case, its similarity to the measured one is striking. In both cases, the calculations explain the observed resonances nearest threshold as $T_<$. For the ^{10}Be* case, the model predicts overlapping $T_>$ states where we know they must be.

We therefore conclude that the states in question have the spin and parity of the IAS but are the isospin antiparallel configurations ($T_<$). Unlike the isobaric analog state ($T_>$), the anti-analog state concept has not provided much insight. Owing to its highly fractured nature, it can even be considered a naive concept. However, in the context of understanding the nature of states just above proton thresholds—states with an outsized importance in the study of the interplay between structure and reactions—this concept has turned out to be useful. The uncollectivized splinters of the AAS in the shell model provide multiple opportunities (a veritable comb of SM states), of which one or more can be ushered by continuum-mediated mixing of SM states into true physical states very close to the proton threshold. In the cases studied here, this mixing is enhanced by open neutron channels. The observable effect of the open neutron channels is to greatly increase the width of the resonances. In the calculations, the quantifiable effect of the neutron channels is to pull the energy window for collectivization down closer to the charged-particle threshold.

The importance of near-threshold, 'fortuitously" placed resonances in nucleosynthesis is well known. However, it has been the recent study of resonances off of synthetic paths, in fact often in truly exotic nuclei (examples being ^{11}Li, ^{15}F, and ^{26}O [17,37,38]), that has generated considerable insight into the effects which generate near-threshold resonances. Specifically, continuum-cognizant shell models have illustrated how the coupling to the continuum generates states with an imprint of the decay channel [17]. The present work adds to, but also complicates, our understanding of this process by which resonances are ushered to decay thresholds by providing examples where the imprinting of a charged-particle channel is aided by open neutron channels.

ACKNOWLEDGMENTS

L.G.S. would like to acknowledge discussions with V. Goldberg and G. Rogachev on the nature, and possible significance, of anti-analog states. We are also grateful to W. Nazarewicz for his initial suggestion that the two ends of this collaboration, one experimental and the other theoretical, join forces. This work is supported in part by the COPIN and COPIGAL French-Polish scientific exchange programs and by the U.S. Department of Energy, Division of Nuclear Physics, under Grant No. DE-FG02-87ER-40316.

[1] F. Hoyle, Astrophys. J. Suppl. Ser. **1**, 121 (1954).
[2] J. D. Barrow and F. J. Tipler, *The Anthropic Cosmological Principle* (Oxford University Press, Oxford, 1988).
[3] E. Epelbaum, H. Krebs, T. A. Lähde, D. Lee, and U.-G. Meißner, Phys. Rev. Lett. **110**, 112502 (2013).
[4] R. J. Charity, S. A. Komarov, L. G. Sobotka, J. Clifford, D. Bazin, A. Gade, Jenny Lee, S. M. Lukyanov, W. G. Lynch, M. Mocko, S. P. Lobastov, A. M. Rogers, A. Sanetullaev, M. B. Tsang, M. S. Wallace, R. G. T. Zegers, S. Hudan, C. Metelko, M. A. Famiano, A. H. Wuosmaa, and M. J. van Goethem, Phys. Rev. C **78**, 054307 (2008).
[5] N. Michel, W. Nazarewicz, M. Płoszajczak, and K. Bennaceur, Phys. Rev. Lett. **89**, 042502 (2002).
[6] R. Id Betan, R. J. Liotta, N. Sandulescu, and T. Vertse, Phys. Rev. Lett. **89**, 042501 (2002).
[7] N. Michel, W. Nazarewicz, M. Płoszajczak, and J. Okołowicz, Phys. Rev. C **67**, 054311 (2003).
[8] T. Berggren, Nucl. Phys. A **109**, 265 (1968).
[9] J. Okołowicz, M. Płoszajczak, and I. Rotter, Phys. Rep. **374**, 271 (2003).
[10] A. Volya and V. Zelevinsky, Phys. Rev. C **74**, 064314 (2006).
[11] H. Feshbach, Ann. Phys. (NY) **5**, 357 (1958); **19**, 287 (1962).
[12] C. Mahaux and H. A. Weidenmüller, *Shell Model Approach to Nuclear Reactions* (North-Holland, Amsterdam, 1969).
[13] P. Kleinwächter and I. Rotter, Phys. Rev. C **32**, 1742 (1985).
[14] S. Drożdż, J. Okołowicz, M. Płoszajczak, and I. Rotter, Phys. Rev. C **62**, 024313 (2000).
[15] N. Auerbach and V. G. Zelevinsky, Rep. Prog. Phys. **74**, 106301 (2011).
[16] N. Michel, W. Nazarewicz, and M. Płoszajczak, Phys. Rev. C **82**, 044315 (2010).
[17] J. Okołowicz, M. Płoszajczak, and W. Nazarewicz, Prog. Theor. Phys. Suppl. **196**, 230 (2012).
[18] J. Okołowicz, W. Nazarewicz, and M. Płoszajczak, Fortschr. Phys. **61**, 66 (2013).
[19] J. Okołowicz, W. Nazarewicz, and M. Płoszajczak, Acta Phys. Pol. B **45**, 331 (2014).
[20] A. Lev, W. P. Beres, and M. Divadeenam, Phys. Lett. B **47**, 408 (1973).
[21] R. J. Philpott, Nucl. Phys. A **179**, 113 (1972).
[22] M. S. Wallace, M. A. Famiano, M.-J. van Goethem, A. M. Rogers, W. G. Lynch, J. Clifford, F. Delaunay, J. Lee, S. Labostov, M. Mocko, L. Morris, A. Moroni, B. E. Nett, D. J. Oostdyk, R. Krishnasamy, M. B. Tsang, R. T. de Souza, S. Hudan, L. G. Sobotka, R. J. Charity, J. Elson, and G. L. Engel, Nucl. Instrum. Methods A **583**, 302 (2007).

[23] G. L. Engel, M. Sadasivam, M. Nethi, J. M. Elson, L. G. Sobotka, and R. J. Charity, Nucl. Instrum. Methods A **573**, 418 (2007).
[24] A. M. Lane and R. G. Thomas, Rev. Mod. Phys. **30**, 257 (1958).
[25] E. Uberseder, G. V. Rogachev, V. Z. Goldberg, E. Koshchiy, B. T. Roeder, M. Alcorta, G. Chubarian, B. Davids, C. Fu, J. Hooker, H. Jayatissa, D. Melconian, and R. E. Tribble, Phys. Lett. B **754**, 323 (2016).
[26] B. Ya. Guzhovsky and L. M. Lazarev, Izv. Akad. Nauk SSSR, Ser. Fiz. **54**, 2244 (1990) [Bull. Acad. Sci. USSR, Phys. Ser. **54**, 156 (1990)].
[27] J. K. Smith, T. Baumann, J. Brown, P. A. DeYoung, N. Frank, J. Hinnefeld, Z. Kohley, B. Luther, B. Marks, A. Spyrou, S. L. Stephenson, M. Thoennessen, and S. J. Williams, Nucl. Phys. A **940**, 235 (2015).
[28] J. Hooker, G. J. Rogachev, V. Z. Goldberg. E. Koshchiy, B. T. Roeder, H. Jayatissa, C. Magana, S. Upadhyayula, E. Uberseder, and A. Saastamoinen, Phys. Lett. B **769**, 62 (2017).
[29] W. Benenson and E. Kashy, Rev. Mod. Phys. **51**, 527 (1979).
[30] J. Jänecke, in *Isospin in Nuclear Physics*, edited by D. H. Wilkinson (North-Holland, Amsterdam, 1969), p. 299.
[31] R. J. Charity, L. G. Sobotka, K. Hagino, D. Bazin, M. A. Famiano, A. Gade, S. Hudan, S. A. Komarov, Jenny Lee, S. P. Lobastov, S. M. Lukyanov, W. G. Lynch, C. Metelko, M. Mocko, A. M. Rogers, H. Sagawa, A. Sanetullaev, M. B. Tsang, M. S. Wallace, M. J. van Goethem, and A. H. Wuosmaa, Phys. Rev. C **86**, 041307(R) (2012).
[32] K. Bennaceur, F. Nowacki, J. Okołowicz, and M. Płoszajczak, Nucl. Phys. A **671**, 203 (2000).
[33] J. Rotureau, J. Okołowicz, and M. Płoszajczak, Nucl. Phys. A **767**, 13 (2006).
[34] J. Okołowicz, M. Płoszajczak, and Yan-an Luo, Acta Phys. Pol. B **39**, 389 (2008).
[35] C. Yuan, T. Suzuki, T. Otsuka, F. Xu, and N. Tsunoda, Phys. Rev. C **85**, 064324 (2012).
[36] See Supplemental Material at http://link.aps.org/supplemental/10.1103/PhysRevC.97.044303 for the wave function decompositions of the states considered in this work.
[37] F. de Grancey A. Mercenne, F. de Oliveira Santos, T. Davinson, O. Sorlin, J. C. Angélique, M. Assié, E. Berthoumieux, R. Borcea, A. Buta, I. Celikovic, V. Chudoba, J. M. Daugas, G. Dumitru, M. Fadil, S. Grévy, J. Kiener, A. Lefebvre-Schuhl, N. Michel, J. Mrazek, F. Negoita, J. Okołowicz, D. Pantelica, M. G. Pellegriti, L. Perrot, M. Płoszajczak, G. Randisi, I. Ray, O. Roig, F. Rotaru, M. G. Saint Laurent, N. Smirnova, M. Stanoiu, I. Stefan, C. Stodel, K. Subotic, V. Tatischeff, J. C. Thomas, P. Ujić, and R. Wolski, Phys. Lett. B **758**, 26 (2016).
[38] Y. Kondo, T. Nakamura, R. Tanaka, R. Minakata, S. Ogoshi, N. A. Orr, N. L. Achouri, T. Aumann, H. Baba, F. Delaunay, P. Doornenbal, N. Fukuda, J. Gibelin, J. W. Hwang, N. Inabe, T. Isobe, D. Kameda, D. Kanno, S. Kim, N. Kobayashi, T. Kobayashi, T. Kubo, S. Leblond, J. Lee, F. M. Marqués, T. Motobayashi, D. Murai, T. Murakami, K. Muto, T. Nakashima, N. Nakatsuka, A. Navin, S. Nishi, H. Otsu, H. Sato, Y. Satou, Y. Shimizu, H. Suzuki, K. Takahashi, H. Takeda, S. Takeuchi, Y. Togano, A. G. Tuff, M. Vandebrouck, and K. Yoneda, Phys. Rev. Lett. **116**, 102503 (2016).

Correction: The DOE grant number contained an error and was corrected.